Quasi-static shear-compression tests on stone masonry walls with plaster: Influence of load history and axial load ratio

Michele Godio[a], Francesco Vanin[a], Shenghan Zhang[a], Katrin Beyer[a,*]

[a] Earthquake Engineering and Structural Dynamics Laboratory (EESD), School of Architecture, Civil and Environmental Engineering (ENAC), École Polytechnique Fe´de´rale de Lausanne (EPFL), EPFL ENAC IIC EESD, GC B2 495, Station 18, CH-1015 Lausanne, Switzerland

Abstract

This paper describes quasi-static cyclic shear-compression tests on six plastered single-leaf stone masonry walls. Of the six walls, four are tested under different axial load ratios, performing a cyclic load history with two cycles per increasing drift demand. Three are tested under the same axial load ratio but are subjected to different load histories, namely, one monotonic loading, one cyclic loading with two cycles per drift level and one cyclic loading with one hundred cycles per drift level. Stiffness, force capacity and drift measures corresponding to six different limit states of the walls are extracted from each test and the effect of the axial load ratio and of the load history on these parameters is investigated. Changing the axial load ratio on the tested walls confirms findings from previous studies, according to which, with increasing axial load the wall stiffness and the force capacity increase while the ultimate drift decreases. Varying the number of cycles in the applied load history brings new findings, showing that all the drift measures of the walls, especially those corresponding to limit states attained in the post-peak regime, are very sensitive to the number of cycles applied while the stiffness and the force capacity are not. These trends are shown in the paper and compared against code and literature provisions for in-plane loaded walls. One face of each wall is plastered and the damage of the plaster is compared to the damage of the stone and mortar. This information is required when assessing the non-structural damage of the walls.

Keywords: Stone masonry, Cyclic shear-compression test, In-plane loading, Load history, Plaster

1. Introduction

The majority of monuments and historical buildings in European countries are stone masonry structures, which are among the most vulnerable structures when subjected to seismic loading [1]. A good understanding of the mechanical behaviour of stone masonry is therefore crucial for the preservation of the cultural heritage of these countries.

In order to understand the mechanical behaviour of stone masonry walls under seismic loading and to define limit state parameters in terms of drift values, which are required as input for the in-plane assessment of a wall, several series of quasi-static tests have been carried out, as reported in Vanin *et al.* [2]. The majority of these tests are shear-compression tests carried out in the laboratory on walls tested under different static and kinematic boundary conditions. Next to the static and kinematic boundary conditions, the force-displacement behaviour of in-plane masonry walls seems to depend also on the load history to which the walls are subjected during the tests [3]. However, only in two test series on stone masonry [4, 5] and two test series on brick masonry [6, 7] the walls were subjected to different load histories, namely, monotonic and reversed cyclic loading. These studies showed that the ultimate drift of walls subjected to monotonic loading is approximately twice as large as the ultimate drift of walls subjected to cyclic loading. A larger ultimate drift for monotonic than for cyclic loading was also observed in the case of reinforced masonry walls [8]. For the seismic assessment of historical buildings, another important yet not much investigated topic is the quantification of drift limits corresponding to the damage of the artistic assets that are

*Corresponding author

Email addresses: michele.godio@epfl.ch (Michele Godio), francesco.vanin@epfl.ch (Francesco Vanin), shenghan.zhang@epfl.ch (Shenghan Zhang), katrin.beyer@epfl.ch (Katrin Beyer)

connected to the structural elements [9, 10]. In order to obtain drift limits corresponding to the onset of damage to the plaster, double-leaf stone masonry walls coated with traditional plaster were tested under diagonal compression and shear-compression [11, 9, 10].

This paper complements previous experimental studies by presenting an experimental programme carried out at the École Polytechnique Fédérale de Lausanne (EPFL) to study the force-displacement behaviour of plastered stone masonry walls under shear-compression loading. The walls tested in the campaign are constructed using squared sandstone blocks arranged in a running bond pattern. According to the classification included in the Italian technical standard [12], the tested walls can be classified as 'dressed rectangular stone masonry with non-soft stones', which is named typology E in Kržan *et al.* [9] and Vanin *et al.* [2]. The experimental programme comprises tests on six walls. The aim of this programme is to investigate the influence of the axial load ratio and the load history on the in-plane stiness, strength and drift parameters of the walls. To this purpose, four of the six walls are tested under dierent axial load ratios, applying a cyclic load history with two cycles per increasing drift level; and three walls are tested under the same axial load ratio but are subjected to dierent load histories, namely, one monotonic loading and two cyclic load histories. With respect to the previous studies, the influence of the load history on the wall behaviour is here studied not only by comparing the monotonic to the cyclic loading but also by investigating the influence of the number of cycles applied during the cyclic loading. For this purpose, cyclic load histories with 2 and 100 cycles per drift level are applied.

The experimental campaign confirms findings from previous studies, showing that with increasing axial load, the wall stiness and force capacity increase while the ultimate drift decreases (see [5, 4, 13, 14, 15] among others). In addition, it brings new findings, highlighting that all drift measures, especially those corresponding to limit states measured in the post-peak regime, are aected by the load history, while the stiness and the force capacity are not. Moreover, the walls are tested up to the loss of vertical load-bearing capacity, which allows determining the drift corresponding to the wall collapse limit state, for which the least amount of data is available for in-plane loaded stone masonry walls [2]. Finally, one side of each wall is plastered, while on the other side the stone masonry is left visible. The comparison of the crack patterns on the plastered and unplastered sides allows establishing correlations between the onset of cracking in the plaster with the cracking in the stone masonry. This information is required when assessing the non-structural damage of the walls [9].

The paper is organised in four sections. Section 2 presents the experimental test programme and gives a description of the test units, material properties, test setup, applied instrumentation, testing procedure and loading protocol. Section 3 shows the experimental test results in terms of response envelopes, their bi-linear idealisations, failure modes of the walls and cracking pattern observed in the plaster. Section 4 discusses the influence of the load history and the axial load ratio on the stiness, force and drift parameters of the force-displacement response of the walls and cracking of the plaster. Section 5 compares the experimental findings with current code and literature provisions for the evaluation of the in-plane response of stone masonry walls.

2. Experimental test programme

The experimental test programme consisted of six quasi-static shear-compression tests made on stone masonry walls with one face plastered (Table 1). Out of the six walls, four were tested under dierent axial load ratios but following the same load history (SC1-SC5). Three walls were tested under dierent load histories but under the same axial load ratio (SC5-SC7); of these three walls, two were tested under two dierent cyclic load histories (SC5-SC6) and one was subjected to a monotonic loading (SC7). In one test (SC2), technical issues with the horizontal actuator prevented the full post-peak behaviour of the wall to be recorded; the experimental results for that test will be nonetheless considered valid for investigating the wall behaviour and they will be therefore presented in Section 3. Another wall (SC3) was tested using the same configuration as SC2, but further issues with the horizontal actuator prevented the test to be carried out and no data is available for this test. All the walls were tested in fixed-fixed conditions, i.e. imposing throughout the test a double-bending moment profile by controlling the actuators in such a way that the height of zero moment was always at mid-height of the wall. The following sections describe the test units (Section 2.1), the material properties of the mortar, the stone and the plaster as well as of the masonry (Section 2.2), the test setup (Section 2.3), the instrumentation (Section 2.4), the test procedure (Section 2.5) and the loading protocols (Section 2.6).

Table 1: Shear-compression tests carried out as part of the experimental programme.

Test	H_w (mm)	L_w (mm)	t_w (mm)	End conditions	N (kN)	σ_v/f_{cm} (%)	Load history*
SC1	900	900	200	fixed-fixed	134	7.5	*LH*1
SC2**	900	900	200	fixed-fixed	178	10.0	*LH*1
SC4	900	900	200	fixed-fixed	273	15.0	*LH*1
SC5	900	900	200	fixed-fixed	207	11.5	*LH*1
SC6	900	900	200	fixed-fixed	207	11.5	*LH*2
SC7	900	900	200	fixed-fixed	207	11.5	monotonic

*Load histories *LH*1, *LH*2 are illustrated in Fig. 4
**partial data available in post-peak behaviour of the wall

(a) (b) (c)

Figure 1: Test units: (a) photo of the test units showing one plastered and one unplastered side; (b) side view on the stonework; (c) side view on the plastered face of a wall.

2.1. Test units

The six stone masonry walls tested as part of the experimental programme had height H_w = 900 mm, length L_w = 900 mm and thickness t_w = 200 mm, excluding the plaster thickness (Fig. 1). The walls were built using squared sandstone blocks from the quarry Büchel in Balzers, Lichtenstein. The stones, of density 2688 kg/m^3 and porosity 7%, were laid at alternate stretcher courses following an almost regular running bond stonework. The stones covered the entire thickness of the walls (single leaf walls); their length varied between 150 and 200 mm and their height between 110 and 140 mm. The head and the bed joints were filled with mortar layers of thickness e_m between 10 and 25 mm (Fig. 1(b)). A cement-free lime-based mortar with a volume ratio of sand to hydraulic lime (NHL5) of 2.5:1 was used to this purpose. This proportion falls into the aggregate-to-binder ratio of 1:1 to 4:1 usually found in ancient buildings [16]. As aggregate, river sand was used, with a maximum aggregate size of 4 mm. One of the wall faces was plastered by applying two layers of plaster. The first layer, denoted with P1, consisted of a plaster made up of three parts of sand and two parts of binder and was applied directly on the wall face, with a thickness varying between 10 and 30 mm depending on the planarity of the wall face (Fig. 1(b)). The external layer, denoted with P2, consisted of a plaster layer that was 5 to 10 mm thick with a sand-to-binder ratio of 1:2. Both layers had a maximum aggregate size of approximately 2 mm. The presence of two plaster layers is frequently found in existing buildings and reported in historical architectural treatises [17]: the first layer is used to obtain a plane surface, while the second layer has enhanced mechanical properties and a lower porosity, which improve its durability. For this test series, the commercial binder 'Mapei-Antique Intonaco' was used for both plaster layers. This is a cement-free pre-blended binder made from natural hydraulic lime (NHL) mixed with Eco-Pozzolan, natural sand, special admixtures and micro-fibres, which was developed by the producer to match mechanical properties and porosity of slurry made of lime, lime-pozzolan and hydraulic lime originally used in the construction of old buildings. The plaster was applied to the entire surface of the walls (Fig. 1(c)).

2.2. Material properties

The shear-compression tests were carried out one and a half years after the construction of the walls. In the same period of the shear-compression tests, material tests were carried out in order to determine the material properties of the constituents, i.e. mortar, stones and plaster, as well as of masonry as a whole. For the mortar, the stone and the two plaster layers the elastic modulus E, the compressive strength f_c and the flexural tensile strength f_{ft} were determined while for the masonry only the elastic modulus E and the compressive strength f_c were established. The results of these tests are summarized in Table 2.

The material tests on mortar and plaster were carried out following the European Standard EN-1015 [18]. The flexural strength was obtained from three-point bending tests performed on prisms of dimensions 40 40 160 mm^3, assuming a linear stress distribution over the prism height at the peak force, from which the flexural tensile strength was derived. The compressive strength was obtained as the maximum vertical stress from simple compression tests performed on the specimen halves resulting from the bending tests. From the simple compression tests, the elastic modulus of mortar and plaster was derived as the stiness between 1/3 and 2/3 of the compressive strength.

The material tests on sandstone consisted in three-point bending and simple compression tests, which were carried out on 40 40 160 mm^3 prisms and 55 55 110 mm^3 cylinders, respectively. During the simple compression tests, three consecutive unloading/reloading cycles were performed at approximately 1/4, 1/2 and 3/4 of the peak force, allowing the elastic modulus of the sandstone to be obtained by fitting straight lines to the unloading/reloading branches of the stress-strain curve and averaging the three values. Following the International Standards ASTM D7012-10 [19], a Poisson ratio of 0.14 was calculated for the sandstone from the transverse deformation of the cylinders.

In addition to the material tests on sandstone, mortar and plaster, two stone masonry walls of size H_w L_w t_w = 900 780 200 mm and a wall of 780 780 200 mm of the same typology than those tested under shear-compression were tested respectively under simple compression and diagonal compression. Simple compression tests were carried out under boundary conditions which limited the lateral confinement eect on the walls. This was achieved by means of an ad hoc system of small movable plates located at the wall top and bottom, allowing the wall ends to be loaded vertically but to move in the horizontal directions with a minimum of restraint. From these tests, the elastic modulus and compressive strength of the masonry were determined. The elastic modulus was extracted from the vertical force-displacement curve of the wall, by fitting the unloading/reloading cycles performed during the tests prior to reaching the peak force. The displacement used for plotting the force-displacement curves corresponds to the relative displacement measured over a base length that covered 6 units and 6 mortar layers, covering almost the entire wall height and excluding the mortar layers at the top and bottom of the wall. This displacement was tracked by a stereo camera system and post-processed by a Digital Image Correlation (DIC) software. The compressive strength f_{cm}, derived by dividing the peak vertical force by the wall cross section, was used to choose the axial load ratios to be used in the shear-compression tests (Table 1). From the diagonal compression test, an estimate of the tensile strength of the masonry of 0.11 MPa was obtained from the measure of the peak compression force P, as [20]: $f_t = P/(2H_w t_w)$.

Based on the results of the material tests and the geometric properties of the test units such as the size and shape of the stones, the number of leaves and the degree of interlocking of the stones, a Masonry Quality Index of 9 has been assigned to the tested stone masonry walls according to the methodology outlined by Borri *et al.* [21].

Table 2: Material properties of the stone masonry walls.

Material	E (MPa)	f_c (MPa)	f_{ft} (MPa)
Sandstone	16900 □ 2731 (16%)	65.60 □ 3.98 (6%)	7.14 □ 1.07 (14.9%)
Mortar	323 □ 65 (20%)	4.08 □ 0.85 (21%)	0.96 □ 0.25 (26%)
Plaster P1 (1st layer)	153 □ 67 (44%)	1.27 □ 0.50 (39%)	0.45 □ 0.22 (48%)
Plaster P2 (2nd layer)	218 □ 51 (23%)	1.80 □ 0.41 (23%)	0.58 □ 0.08 (14%)
Masonry	5328 □ 924 (17%)	10.34 □ 2.20 (21%)	-

Notation: Mean □ St. Dev. (C.o.V.)

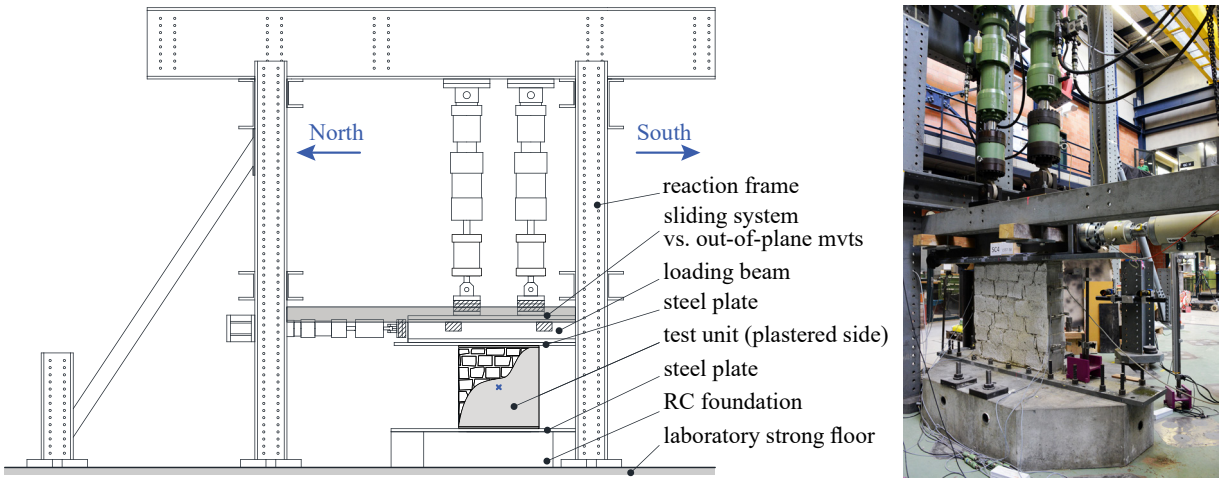

(a) (b)

Figure 2: Test setup used for the tests at the École Polythecnique Fédérale de Lausanne (EPFL): (a) illustrative sketch, front view on the plaster side; (b) side view on the masonry side.

2.3. *Test setup*

Fig. 2 illustrates the test stand in which the shear-compression tests were carried out. The test units were built outside the test stand and were lifted into the test stand one at a time by means of a forklift. In the stand, they were laid on a 35-mm thick steel plate bolted to a 400-mm high reinforced-concrete foundation which was, in turn, fixed to the laboratory strong floor by means of post-tensioned steel bars. The upper surface of the steel plate was roughened by a thin layer of quarzitic sand glued with expoy to the steel plate, which oered su□cient friction to prevent sliding between the wall base and the steel plate. Another steel plate was prepared in the same manner and placed on top of the wall together with the steel loading beam. Prior to testing, two additional layers of cement-based mortar of thickness 10 to 20 mm were introduced between the steel plates and the test units in order to level the end surfaces of the walls and therefore guarantee a uniform stress transfer between the steel plates and the walls upon load application. Such layers were cured for two to four days before the test, under a constant compression stress of about 0.05 MPa.

Loads were applied to the walls by means of two vertical and one horizontal servo-hydraulic actuators adequately fixed to the steel reaction frame (Fig. 2). During the test, the load was applied on the upper face of the wall and not directly on the plaster. An auxiliary sliding system was put in place in order to prevent any out-of-plane movements of the wall. The system consisted of four short timber beams which, at one end, were bolted to a L-shaped steel profile (shown with transparency in Fig. 2(a)) and, at the other end, were in contact with the web of the loading beam; friction between the web and the short beams was minimised through the use of a Teflon sheet and a layer of grease.

2.4. *Measurements*

During the tests, the walls were instrumented in order to measure the following quantities (Fig. 3): (a) the forces applied by the three actuators, denoted with $F_{act,h}$; $F_{act,v1}$; $F_{act,v2}$ and measured by load cells inside the actuators; (b) the displacements of the three actuators, u_{act}; $v_{act,1}$; $v_{act,2}$, used to control the actuators and measured by the transducers inside the actuators; (c) the horizontal displacement of the center line of the loading beam, u_{lb}, used to monitor the drift demand applied during the test and measured by means of two LVDTs on the south end of the loading beam; (d) two vertical displacements of the loading beam, $v_{ls,1}$ and $v_{ls,2}$, obtained from two laser sensors positioned below the beam on the south and north sides of the walls (indicated with red dashed lines in Fig. 3) and used to derive the vertical displacement of the loading beam $v_{lb} = v_{ls,1} + v_{ls,2} =2$ and its rotation about the out-of-plane axis $!_{lb} = v_{ls,1} \; v_{ls,2} =2$; (e) the change in wall thickness, $_{t,t}$, $_{t,c}$, $_{t,b}$, measured by two sets of horizontal LVDTs placed on the north and south wall faces at three dierent heights (top, center, bottom) fixed to the stones; the base length of these LVDTs was approximately 2/3 of the wall thickness.

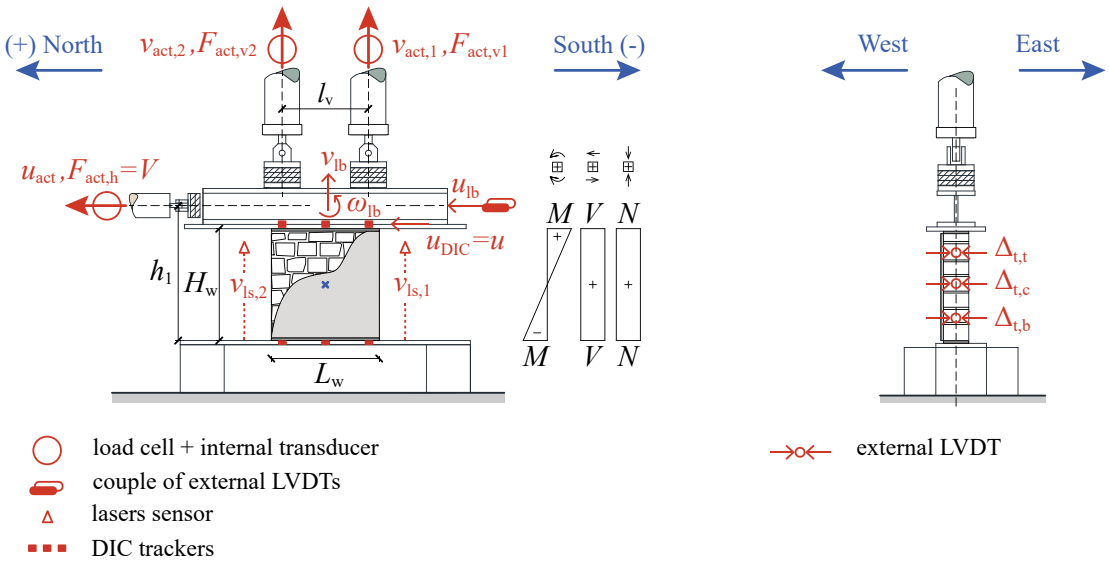

Figure 3: Measurements and conventions adopted in the test procedure: geometry, forces, displacements and distributions of bending moment *M*, shear force *V* and axial force *N*.

In addition to the above mentioned hard-wired measurements, the 3D deformation fields of the east and west wall faces were measured through two stereo camera vision systems using the DIC software Vic-3D 7 [22]. For this purpose, the faces of the walls were painted in white and covered with a random black speckle pattern. In order to measure the out-of-plane deformation, each pair of cameras was placed in front of the wall faces with an angle of □20□. Three squares of white paper with black speckle were glued to both sides of the bottom flange of the loading beam and near the top edge of the concrete foundation. The horizontal displacement of the loading beam tracked by the DIC system was computed as the average of the displacements of the three squares on the east side of the loading beam and is denoted with u_{DIC} (Fig. 3). This measurement is used for plotting the final horizontal force-displacement curves shown in this paper, where the horizontal displacement is for simplicity indicated with u.

2.5. Test procedure

The shear-compression tests were performed in two steps. In the first step of the procedure, a vertical force N, which is defined as positive when it applies a compression load on the wall, was applied to the wall by the two vertical actuators. This corresponded to a normal vertical stress $\sigma_v = N/(L_w t_w)$ and to an axial load ratio of σ_v/f_{cm}, which was varied from wall to wall during the experimental programme (Table 1). In the second step of the procedure, the walls were subjected to a quasi-static shear force V, which was exerted by the horizontal actuator following the prescribed loading protocol (Section 2.6). In this phase, the axial force N was kept constant by the vertical actuators and the walls were tested under fixed-fixed static boundary conditions, i.e. ensuring a constant shear span H_0 equal to H_w=2 throughout the test. This boundary condition was obtained by means of a force couple applied by the vertical actuators, which was proportional to the load applied by the horizontal actuator.

In order to guarantee the correct loading and boundary conditions, the three actuators were operated in a coupled mode in both steps of the test procedure. In the first step, the vertical actuators were coupled to each other in order to apply the same amount of vertical force: $F_{act,v1} = F_{act,v2} = N/2$. In this phase, both vertical actuators were operated in a force-controlled mode. The horizontal actuator was also force-controlled in order to keep the horizontal force equal to zero. The forces of the vertical actuators were set to zero when all three actuators were connected to the horizontal beam but the wall not yet in the test stand. In this way, the force and the moment resulting from the self-weight of the horizontal actuator and of the loading beam were balanced by the vertical actuators and did not lead to a bias in the vertical forces. The force of the horizontal actuator had been set to zero before connecting it to the loading beam. In the second step, the horizontal actuator was operated in a displacement-controlled mode and both vertical actuators in a force-controlled mode. Their forces were coupled to the force of the horizontal actuator in

order to apply the correct moment at the top of the wall. The condition of zero moment at the wall mid-height was used to derive the forces exerted by the vertical actuators, which resulted in: $F_{act,v1} = N/2 - F_{act,h}(h_1 - H_w/2)/l_v$ and $F_{act,v2} = N/2 + F_{act,h}(h_1 - H_w/2)/l_v$, with $F_{act,h} = V$ and l_v, h_1 respectively the distance between the two vertical actuators and the position of the horizontal actuator with respect to the foundation (Fig. 3). During the tests, the vertical displacement of the loading beam v_{lb} and its rotation about the out-of-plane axis θ_{lb} were not actively controlled. Keeping the height of zero moment at mid-height of the wall resulted in approximately zero rotation of the loading beam at the beginning of the test. During the last stages of each test, when the walls were heavily damaged, large rotations of the beam could be observed.

2.6. Loading protocol

In the first step of the test procedure, three quasi-static unloading-reloading cycles of vertical force were performed at $N/3$, $2N/3$ and N prior to applying the prescribed axial load N. This allowed the initial elastic stiffness of the walls to be measured under vertical loading conditions and to be compared with the initial stiffness measured from the simple compression tests and from the shear-compression tests, see Section 5.1.

In the second step of the test procedure, the horizontal force was applied, for one wall, in a monotonic way, and, for the rest of the walls, by following quasi-static cycles of increasing drift demand $\delta = u/H_w$ of 0.025, 0.05, 0.1, 0.15, 0.2, 0.25, 0.3, 0.4, 0.5, 0.6, 0.8, 1, 1.5, 2, 2.5, 3 and 4%. To this purpose, two different load histories were set up: the load history *LH*1, consisting of 2 cycles per drift demand, and the load history *LH*2, consisting of 100 cycles per drift demand (Fig. 4). For all loading histories, the applied displacement rate was of 0.01 mm/s in the early stages, up to 0.1 mm/s in the latest stages. As mentioned in Section 2.4, u_{lb} was used for controlling the amplitude and the loading direction during the tests. When applying the load history *LH*2 in the test SC6, the loading beam underwent an increasing in-plane rotation because of the damage to the wall, which, due to the high number of cycles, accumulated since the early stages of the test. This rotation progressively increased u_{lb} starting from 0.25% drift. This bias was removed by plotting the horizontal displacement u_{DIC} instead of u_{lb} in the force-displacement diagrams. The two measurements were not the same because they were measuring the displacement of the loading beam at two different heights. The measurement at the bottom flange of the beam provided by u_{DIC}, which represents more accurately the actual displacement demand on the wall, showed that the actual displacement history applied in that test was increasingly asymmetric.

For all test except SC7, the walls were loaded up to failure of the their vertical load-bearing capacity. The wall SC7 was loaded monotonically until the maximum stroke of the horizontal actuator was reached. At this point, the wall was very close to collapse and the displacement at collapse was therefore set equal to the stroke of the actuator.

3. Experimental test results

This section presents the experimental results in terms of the force-displacement hysteresis curves and their envelopes (Section 3.1). It provides key parameters such as the maximum shear force and drifts for various limit states (Section 3.2) and the stiffness, strength and ultimate drift of a bi-linear approximation of the envelopes (Section 3.3). It further describes the wall failures modes (Section 3.4) and the damage to the plaster (Section 3.5).

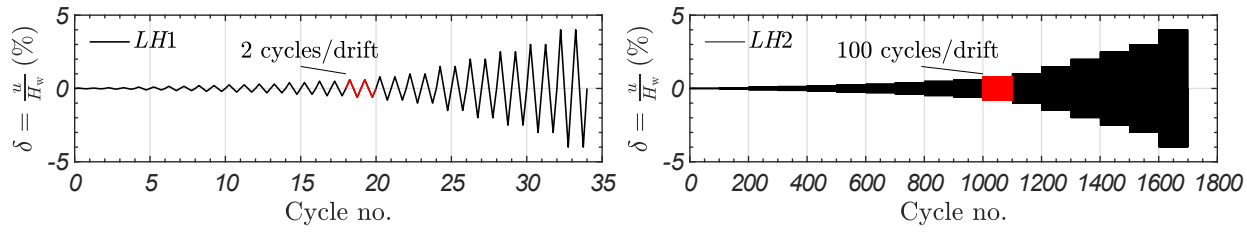

Figure 4: Cyclic load histories used in tests SC1-SC5 (*LH*1) and SC6 (*LH*2). Applied drift demands (%): 0.025, 0.05, 0.1, 0.15, 0.2, 0.25, 0.3, 0.4, 0.5, 0.6, 0.8, 1, 1.5, 2, 2.5, 3, 4.

3.1. Experimental force-displacement response curves and envelopes

Fig. 5 shows the horizontal force-displacement curves obtained from the six accomplished shear-compression tests made on the stone masonry walls. The shear force V is the horizontal force exerted by the horizontal actuator $F_{act,h}$. The horizontal displacement u is the horizontal displacement of the loading beam tracked by the stereo camera system u_{DIC} (Section 2.4). For clarity, the drifts □= u_{DIC}=H_w are also indicated. For the cyclic tests, the experimental force-displacement curves are presented together with their envelope curves. These latter are built starting from the cyclic curves by taking, for each displacement, the force that is measured the first time this displacement is attained. When building the negative envelope, the same procedure is followed except that the envelope of the first cycle is replaced by a straight line connecting the origin to the negative peak displacement of the first cycle. This is done in order to obtain a better estimate of the initial wall stiness derived from the negative envelope.

As stated in Section 2, during the test SC2 a technical issue related to the horizontal actuator occurred when reaching the negative peak at 0.2% drift, preventing the measurement of the post-peak behaviour of the wall between 0.2% and 1% drift. A dotted-dashed line is used in Fig. 5 for the test SC2 to indicate where the data is not available. It is also to notice that during the test SC7, where the wall was subjected to monotonic loading, the test was ended at a drift of more than 12%. At this drift, the stroke of the actuator reached its limit but the wall still maintained its vertical load-bearing capacity.

3.2. Key parameters of the experimental response envelopes

Table 3 and Table 4 summarise the key parameters of the experimental force-displacement response envelopes. Table 3 gives V_{max}, the peak force of the force-displacement envelope, indicating the shear strength of the walls against in-plane loading, and K_{init}, the initial stiness of the walls, computed as the secant stiness at 0.15V_{max} of the envelope curve [2]. Table 4 gives drift measures that correspond to six wall limit states as defined in [9, 2]: □$_{cr}$ is the drift corresponding at the onset of cracking in the masonry, measured when the first crack appeared on the masonry side of the wall and detected by visual inspection of the walls; □$_y$ represents the drift at the yielding point of the bi-linear curve approximating the experimental force-displacement response envelope (Section 3.3); □$_{max}$ is the drift measured when the peak force was reached; □$_{SD}$ is the drift at the Severe Damage (SD) limit state and is defined as □$_{SD}$ = min (3□$_{cr}$; □$_{max}$); □$_u$ is the ultimate drift and corresponds to the displacement attained in the post-peak part of the envelope at 0.80V_{max}; □$_c$ is called drift at collapse, or drift capacity, and is defined here as the maximum drift measured in the cycles prior to loss of the vertical load-bearing capacity of the walls, which determined the end of the tests (Section 2.6). These drift parameters may enter as input to the database for stone masonry walls built by Vanin *et al.* [2]. Note that previous test series were typically stopped before the vertical load bearing capacity was reached. As a proxy for □$_c$, the drift at 50% drop of the peak force was taken [2]. As shown in Section 5.3, the use of the drift at 50% drop of the peak force can lead to an underestimation of the drift capacity of the walls.

For each parameter contained in Table 3 and Table 4, the values obtained from the positive and from the negative envelope curves are given. Moreover, for each test, the average values are given for all parameters except for □$_u$ and □$_c$, for which the minimum absolute value is retained. For the test SC6, the maximum value is retained due to

Table 3: Key parameters of the experimental force-displacement response envelopes: peak force and initial stiness. Values obtained from the positive and the negative envelope curves. Mean and C.o.V. are calculated based on all positive and negative values.

Test	V_{max} (kN)			K_{init} (kN/mm)		
	pos.	neg.	avg.	pos.	neg.	avg.
SC1	74	-77	76	184	177	180
SC2	90	-89	90	207	235	221
SC4	142	-133	138	267	295	281
SC5	113	-107	110	247	216	231
SC6	109	-106	108	226	225	225
SC7	103	-	103	216	-	216
Mean		-			227	
C.o.V.		-			15%	

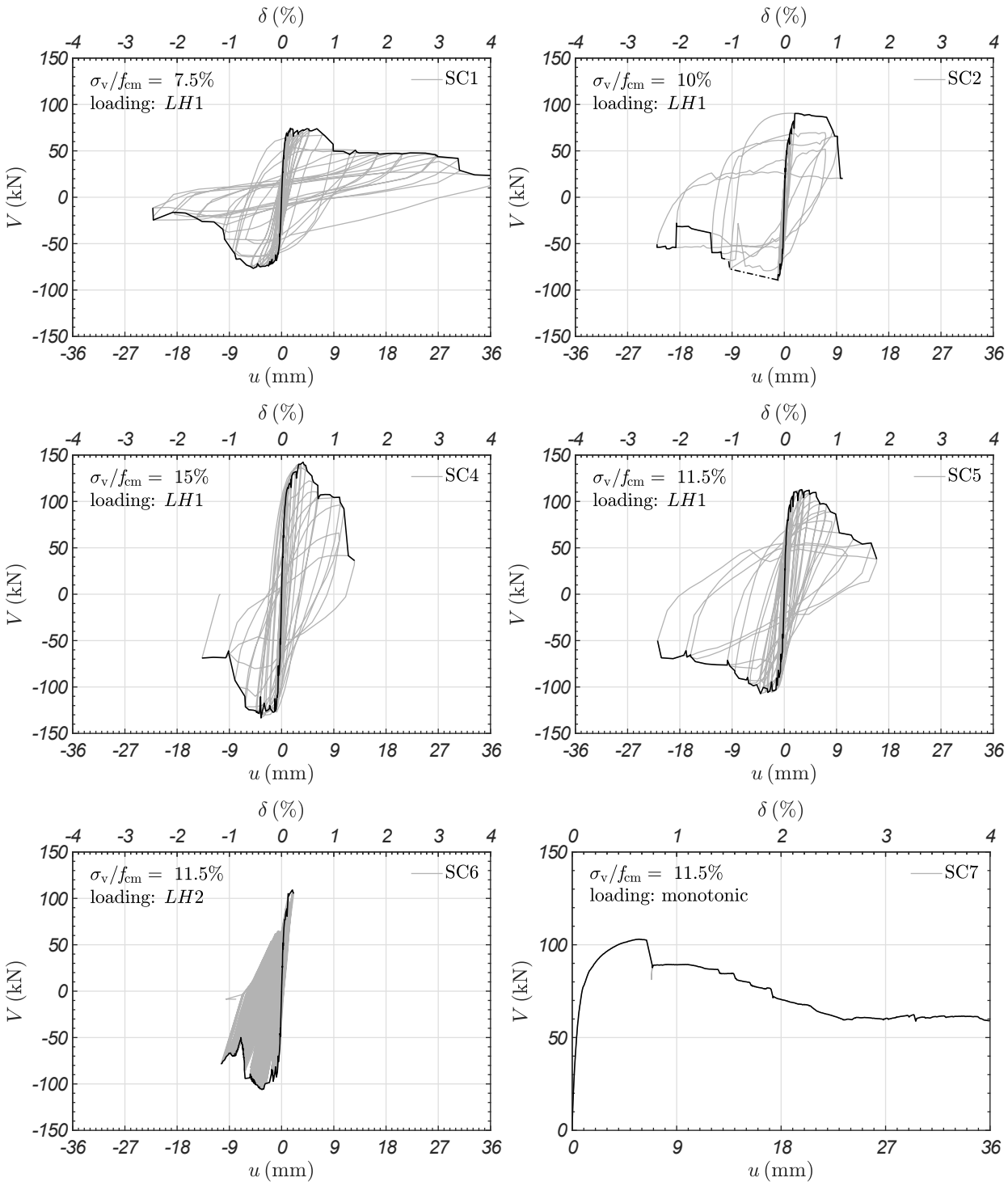

Figure 5: Horizontal force-displacement responsecurves and envelopes.

the asymmetry of the load history followed during this test. The average value of $\square_{SD}$ is evaluated as the minimum between the average of $3\square_{cr}$ and the average of $\square_{max}$. It can be noticed that the values of stiness and peak force

Table 4: Key parameters of the experimental force-displacement response envelopes: drift measures. Mean and C.o.V. are calculated based on all values obtained from the positive and the negative envelope curves.

Test	□cr (%)			□y (%)			□max (%)			□SD (%)			□u (%)			□c (%)		
	pos.	neg.	avg.	pos.	neg.	avg.	pos.	neg.	avg.	pos.	neg.	avg.	pos.	neg.	min.*	pos.	neg.	min.*
SC1	0.11	-0.10	0.11	0.05	-0.05	0.05	0.17	-0.54	0.36	0.17	-0.29	0.32	0.99	-0.90	0.90	4.51	-2.47	2.47
SC2	0.09	-0.08	0.08	0.09	-0.04	0.06	0.20	-0.12	0.16	0.20	-0.12	0.16	0.93	-1.07	0.93	1.12	-2.44	1.12
SC4	0.07	-0.06	0.07	0.08	-0.07	0.07	0.41	-0.39	0.40	0.22	-0.17	0.20	0.70	-0.81	0.70	1.28	-1.52	1.28
SC5	0.11	-0.14	0.13	0.06	-0.07	0.07	0.34	-0.45	0.40	0.34	-0.43	0.39	0.88	-0.95	0.88	1.77	-2.43	1.77
SC6	0.10	-0.12	0.11	0.06	-0.06	0.06	0.21	-0.37	0.29	0.21	-0.35	0.29	0.23	-0.71	0.71	0.23	-1.16	1.16
SC7	0.16	-	0.16	0.09	-	0.09	0.64	-	0.64	0.49	-	0.49	1.56	-	1.56	12.43	-	12.43
Mean		0.10			0.06			0.35			0.27			0.88			2.85	
C.o.V.		30%			24%			46%			43%			36%			118%	

*For SC6, the maximum value is retained due to the asymmetry of the loading protocol

Table 5: Parameters of the bi-linear response envelopes built upon the experimental force-displacement response envelopes.

Test	V_u (kN)	$V_u=V_{max}$	□y(%)	□u(%)	K_e (kN/mm)	$K_e=K_{init}$
SC1	71	0.93	0.05	0.90	120	0.67
SC2	85	0.95	0.06	0.93	126	0.57
SC4	126	0.92	0.07	0.70	151	0.54
SC5	101	0.92	0.07	0.88	130	0.56
SC6	100	0.93	0.06	0.71	148	0.65
SC7	92	0.90	0.09	1.56	93	0.43

obtained from the positive and the negative envelope curves are almost identical (Table 3), which indicates that the test setup did not introduce any bias in the behaviour of the walls.

The variation of the key parameters against the load history and the axial load ratio is discussed in Section 4.1 to Section 4.3. Moreover, since current modelling approaches and code provisions for stone masonry neglect the dependency of the wall parameters on the load history and assume that only the shear strength is dependent on the axial load ratio, Table 3 and Table 4 give, except for the shear strength, the mean values and the C.o.V. values computed from all the tests.

3.3. Parameters of the bi-linear response envelopes

Table 5 contains the parameters of the bi-linear curves approximating the experimental force-displacement envelopes. The bi-linear curves are built as follows: the ultimate drift □u is derived as described in Section 3.2; the eective stiness K_e is the secant stiness at $0.7V_{max}$; the ultimate force V_u is such that the areas below the bi-linear and the experimental envelopes are the same; the yield drift □y is computed as □y = V_u/K_e. Each of these parameters is evaluated both for the positive and for the negative envelope. The resultant curve is finally obtained by taking the average values for V_u and □y and the minimum value for □u. For the test SC6 the maximum value of □u is retained, due to the asymmetry of the loading protocol. The influence of the load history and the axial load ratio on the parameters of the bi-linear curve are discussed in Section 4.4.

3.4. Failure modes of the walls

Fig. 6 shows the failure modes of the walls, showing their deformation state when the ultimate drift □u was reached. As it is visible from the cracking pattern, all the walls underwent shear failure. The failure modes were in fact characterised by marked stair-stepped diagonal cracks, which began to develop at the early stages of the tests and progressively spread from the core of the walls to their corners. The cracks spread mainly through the mortar joints, more particularly at the interface between the blocks and the joints, whereas the stone blocks were cracked only in some limited regions of the walls, especially at the corners. This type of failure mode was expected, given the fixed-fixed boundary conditions under which the walls were tested and the high value of tensile and compressive strength of the sandstone, which prevented the stone blocks from diuse cracking and crushing often observed in brick masonry.

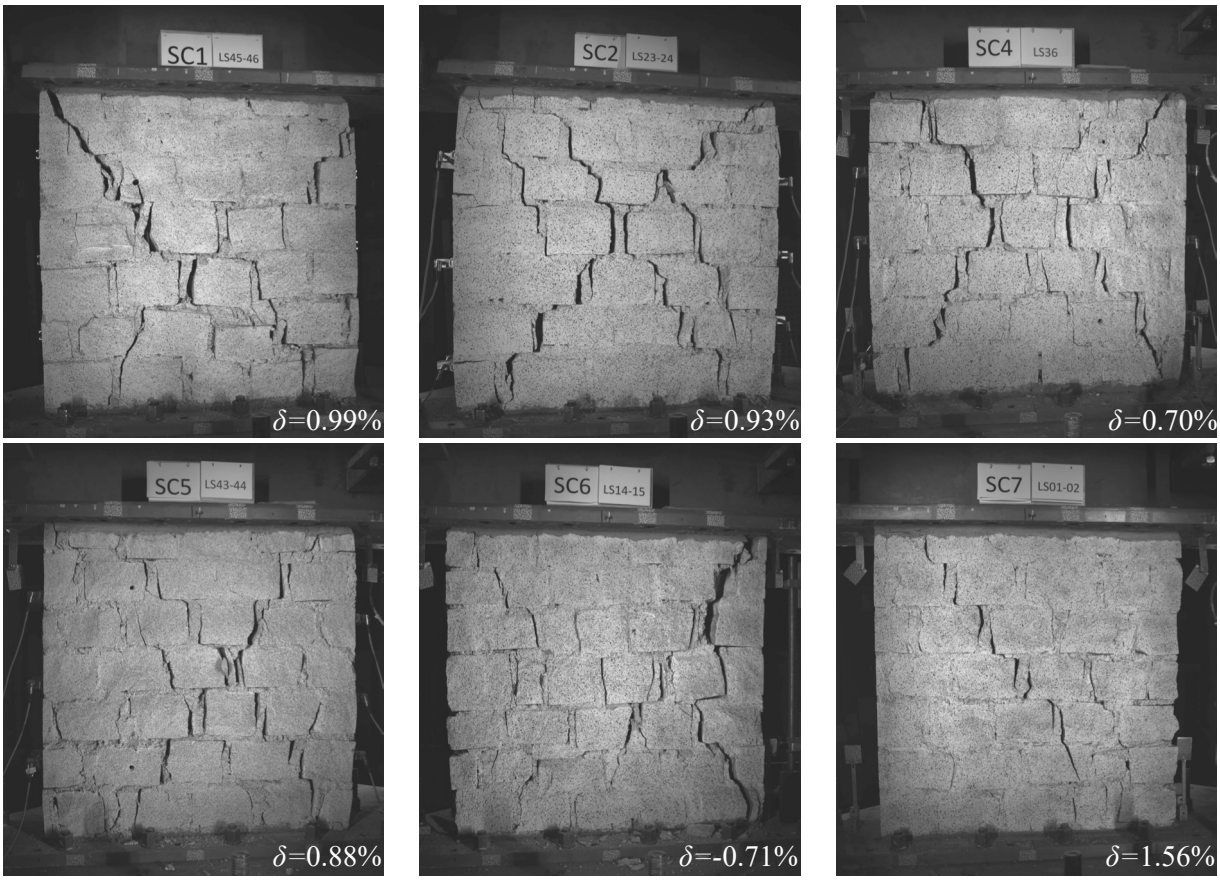

( ) South □ North (+) !

Figure 6: Failure modes of the walls. Pictures taken at the positive (for test units SC1-SC5,SC7) and negative (for SC6) ultimate drift $\square_u$.

3.5. Cracking of the plaster

Fig. 7 illustrates the cracking pattern of the plastered faces of the walls for a level of drift that is between the peak and the ultimate drift. The cracking pattern features several wide diagonal cracks from which minor to hairline cracks propagate. The main diagonal cracks correspond approximately, even though not exactly, to the cracks observed in the masonry (c.f. Fig. 6). The dierence in crack patterns may result from three sources: (i) the irregularity of the stones, which led to dierences in the joint layouts on the two wall sides; (ii) the local detachment of the plaster from the stone in the vicinity of the crack; (iii) the detachment of the second plaster layer from the first plaster layer, which was frequently observed in plaster pieces that fell o the wall. Table 6 gives the drift $\square_{pl}$, which corresponds to the onset of cracking within the plaster as detected by visual inspection, and its ratio with respect to the drift $\square_{cr}$ corresponding to the onset of cracking in the masonry. The variation of these parameters against the axial load ratio and the load history is discussed in Section 4.5.

4. Influence of the axial load ratio and the load history on the wall response

Tests SC1 to SC5 were performed to investigate the influence of the axial load ratio on stone masonry, whereas tests SC5 to SC7 were performed to investigate the influence of the load history on stone masonry (Table 1). The sections below show the eect of changing the load history and the axial load ratio on the parameters of the experimental response envelopes (Section 4.1- Section 4.3), the bi-linear approximation of these envelopes (Section 4.4) and the onset of cracking in the plaster and in the masonry (Section 4.5). Fig. 8 serves as basis for the investigation, oering

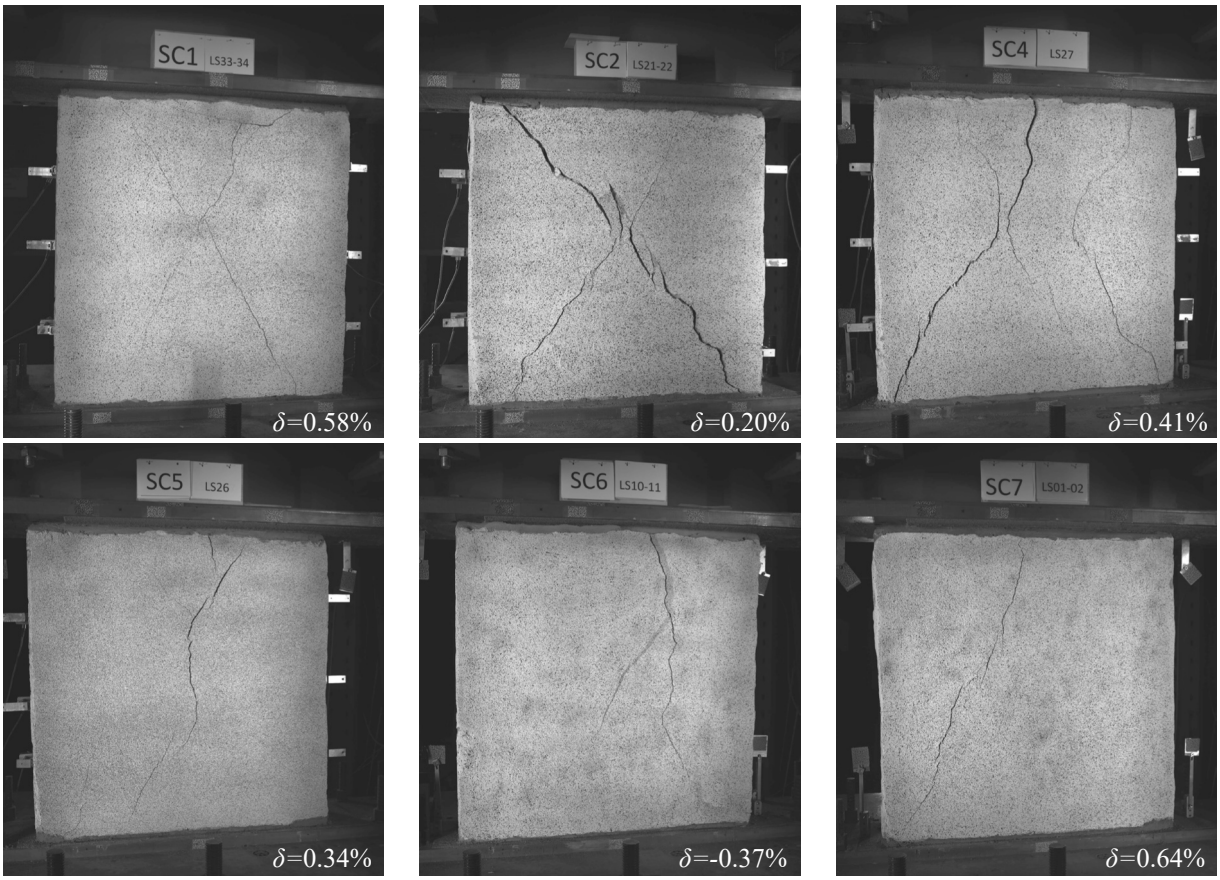

Figure 7: Damage of the plaster. Pictures taken at the positive (for test units SC2-SC5,SC7) and negative (for SC6) peak drift $\square_{max}$. For SC1, the picture at the positive drift ($\square_{max}$+ $\square_u$)=2is shown.

Table 6: Drifts at the onset of cracking in the plaster $\square_{pl}$ and comparison with the cracking in the masonry $\square_{cr}$. Mean and C.o.V. are calculated based on all values obtained from the positive and the negative envelope curves.

Test	$\square_{pl}$ (%)			$\square_{pl}$=$\square_{cr}$		
	pos.	neg.	avg.	pos.	neg.	avg.
SC1	0.11	-0.10	0.11	1.00	1.00	1.00
SC2	0.09	-0.08	0.08	1.00	1.00	1.00
SC4	0.07	-0.06	0.07	1.00	1.00	1.00
SC5	0.11	-0.10	0.11	1.00	0.70	0.85
SC6	0.07	-0.07	0.07	0.64	0.57	0.60
SC7	0.19	-	0.19	1.17	-	1.17
Mean		0.09			0.91	
C.o.V.		39%			21%	

a visual comparison between the experimental force-displacement envelopes resulting from each set of tests. In the figures used for the investigation (Fig. 9-Fig. 12), besides the raw data points, a linear regression curve of the data and the Pearson correlation coe□cient *r* are given when showing the influence of the axial load ratio on the investigated parameters. The correlation coe□cient *r* is a measure of how well the data correspond to the linear regression curve;

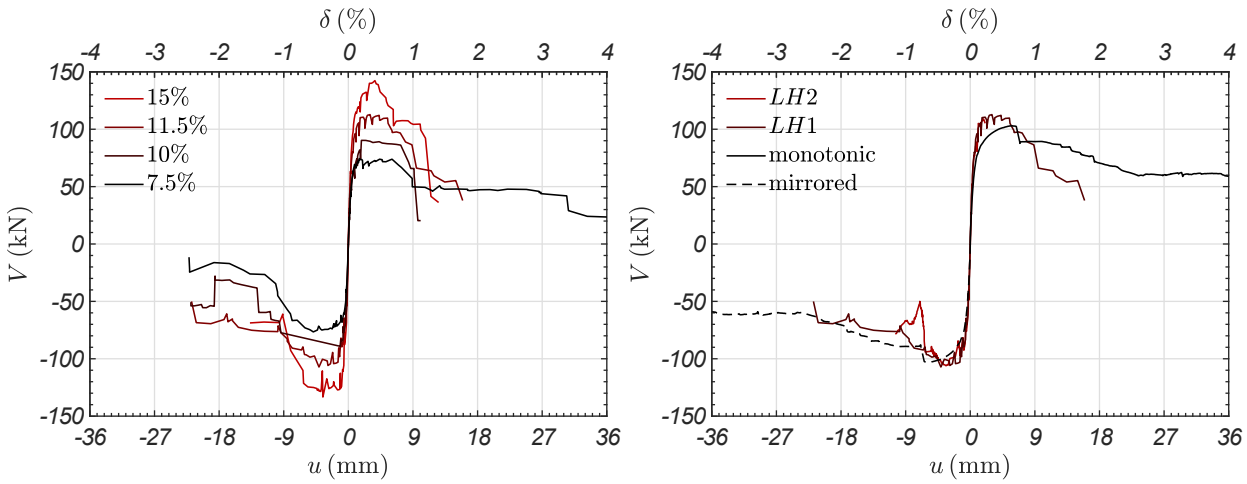

Influence of the axial load ratio $\square_v=f_{cm}$ Influence of the load history

Figure 8: Comparison between experimental force-displacement response envelopes.

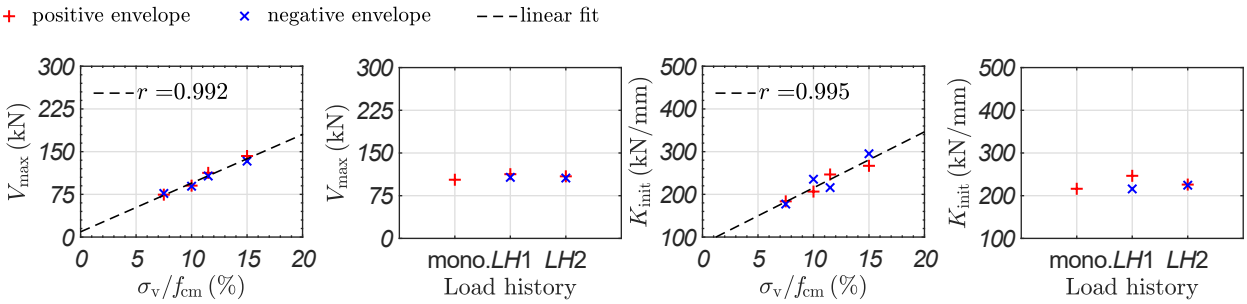

(a) Peak force (b) Initial stiness

Figure 9: Influence of the axial load ratio and of the load history on the peak force (a) and the initial stiness (b) of the experimental force-displacement response envelopes. The corresponding numerical values are listed in Table 3.

the higher the absolute value of r, the better the linear correlation represents the actual data. The purpose of using a linear regression is to better support the experimental observations; the expressions resulting from these regressions are related solely to this experimental campaign or, as discussed in Section 5, to masonry walls with similar characteristics and typology. For a more general discussion on all the masonry typologies, the reader is referred to Vanin *et al.* [2] and Kržan *et al.* [9].

4.1. Influence on the peak force

Fig. 9(a) shows the influence of the axial load ratio and of the load history on the peak force V_{max} of the force-displacement envelopes (Section 3.2). The peak force increases for increasing axial load ratios following a trend that is almost perfectly linear. The load history has, however, no considerable eect on it (Fig. 8).

4.2. Influence on the initial stiness

Fig. 9(b) shows the influence of the axial load ratio and of the load history on the initial stiness K_{init} of the force-displacement envelopes. The initial stiness follows nearly the same trend as the peak force, i.e., it increases linearly with the axial load ratio but is not significantly influenced by the load-history.

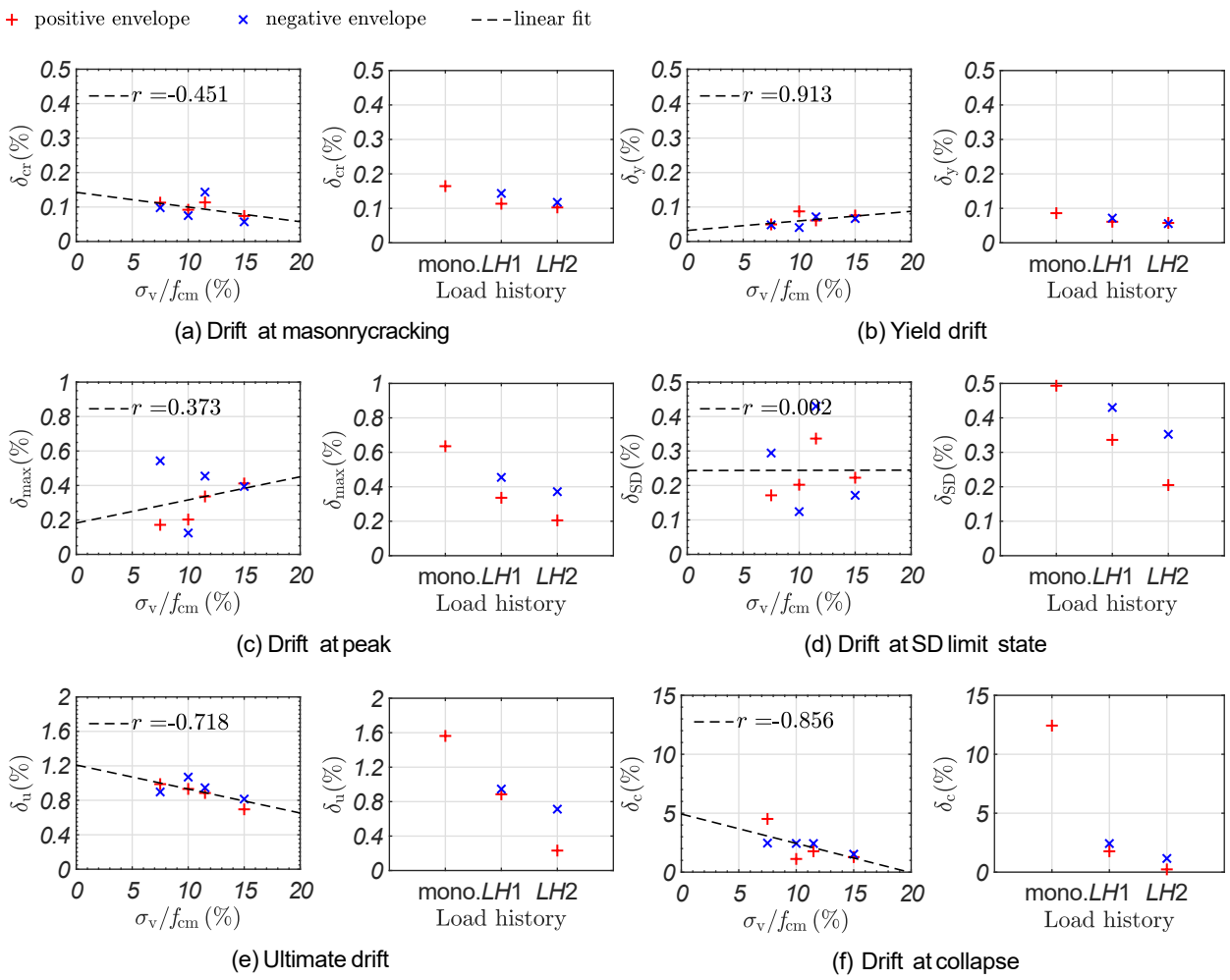

Figure 10: Influence of the axial load ratio and of the load history on the drifts of the experimental force-displacement responseenvelopes. The corresponding numerical values are listed in Table 4.

4.3. Influence on the drifts

Fig. 10 shows the influence of the axial load ratio and of the load history on the drifts corresponding to the six limit statesintroduced in Section 3.2. Focusing on the influence of the axial load ratio, the two drifts measuredin the post-peak regime, $\delta_u$and δ_c,sensibly decreasewith increasing axial load, while for δ_{cr}, $\delta_{max}$and $\delta_{SD}$the influence of the axial load is less strong and clear. The yield drift $\delta_y$is the only drift that showsa positive trend with the axial load ratio. This drift measureis not linked to a physical limit statebut is the result of the bi-linear approximation of the force-displacement curve, suggestingthat the axial load ratio hasa stronger eect on the shearforce capacity than on the eective stiness (Fig. 9). With regard to the influence of the numberof cycles on the drifts, the picture is more homogeneousthan for the influence of the axial load ratio: all drifts decreasewith increasing number of repeated cycles. In particular, for eachof the drifts measuredin the pre-peak regime, δ_{cr}, δ_y, $\delta_{max}$and δ_{SD}, the drift reached under monotonic loading is approximately twice as large asthe drift attained when the load history with 100 cycles is applied (*LH*2) while the load history with 2 cycles (*LH*1) leadsto intermediate values. For the drifts measuredin the post-peak regime, $\delta_u$and δ_c, the sensitivity to the load history is stronger, with the largest dierence occurring betweenthe drifts at collapseundermonotonic loading andcyclic loading, which dier by afactor of 7. This is mainly due to the large amount of accumulated damagethat a cyclic reversed protocol causesto the masonry throughout the test (Fig. 6). Under cyclic loading cracking occurred along the two wall diagonals and the zonewhere the two cracks

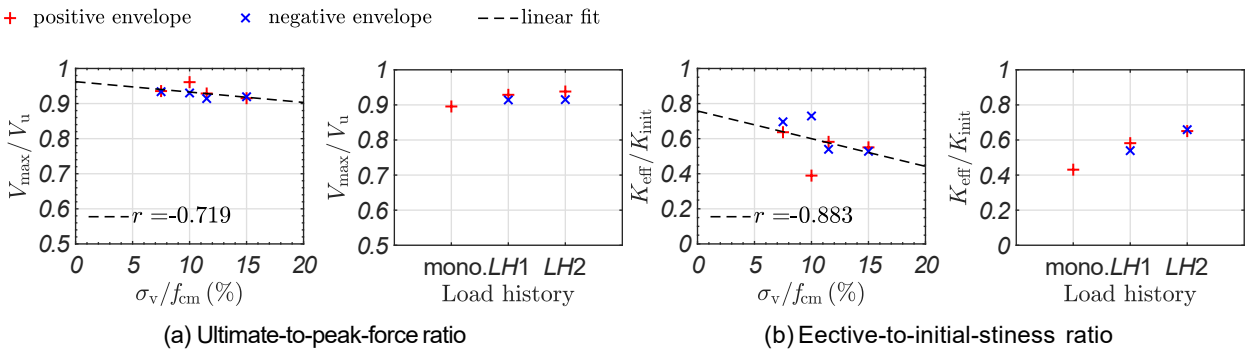

(a) Ultimate-to-peak-force ratio (b) Eective-to-initial-stiness ratio

Figure 11: Influence of the axial load ratio and of the load history on the parametersof the bi-linear force-displacement responseenvelopes. The corresponding numerical values are listed in Table 5.

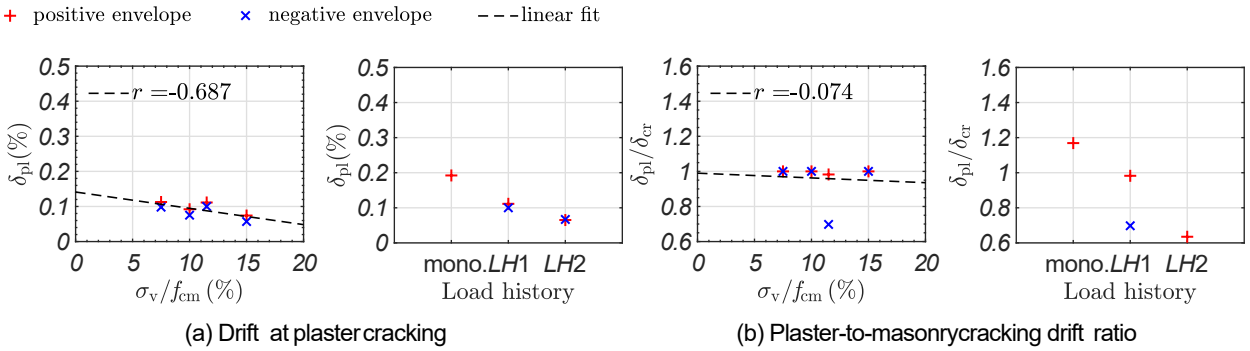

(a) Drift at plaster cracking (b) Plaster-to-masonrycracking drift ratio

Figure 12: Influence of the axial load ratio and of the load history on the cracking of plaster. The corresponding numerical values are listed in Table 6.

intersected was heavily damaged. Such a zone did not exist under monotonic loading and the wall collapse occurred becauseof a large sliding displacement in the bed joints localized along the diagonal crack.

4.4. Influence on the parameters of the bi-linear envelopes

Fig. 11 shows the influence of the axial load ratio and the load history on the parametersof the bi-linear response envelopesof the walls, with regard to (a) the ultimate-to-peak force ratio V_u=V_{max} and (b) the eective-to-initial stiness ratio K_e=K_{init}. The ultimate-to-peak force ratio decreasesforincreasing axial load ratios and increaseswhen moving from the monotonic to the cyclic load histories. Nonetheless, the variation is rather limited and the average value, calculatedbasedonall tests, is 0.92 with a C.o.V. of 2%. The eective-to-initial stiness ratio follows a similar trend but with a larger variation: its value rangesfrom 0.40 to 0.80 with an averagevalue of 0.57 and C.o.V. of 15%. The increaseof stiness ratio that is obtained by varying the load history results from the definition of the envelope curve: when the number of cycles increasesin the load history, the reversedbranchesof the force-displacement curve intersect the *V*-axis at higher levels and the envelopecurve is thus stier.

4.5. Influence on the cracking of the plaster

Fig. 12 shows how, moving from low to high axial load ratios and from monotonic to cyclic load histories, the onset of cracking in the plaster occurs for lower drift values (Fig. 12(a)). Moreover, the more cycles are applied per drift level, the smaller the ratio of the drift at which cracking in the plaster first occurred to the drift at which cracking in the masonry first occurred (Fig. 12(b)); the axial load ratio seemsto haveno eect on this phenomenon.

The drift values obtained for □$_{pl}$ are in line with previous test results obtained from masonry walls of typology E failing in shear[10], for which the drift corresponding to the first onset of cracking in the plaster occurs for 0.05 to 0.10% [9].

5. Comparison with code and literature provisions for in-plane loaded walls

This section resumes the main experimental findings and compares them with code and literature provisions for in-plane loaded stone masonry walls. The comparison is with regard to the prediction of the stiness (Section 5.1), force capacity (Section 5.2) and drift limits (Section 5.3) of the walls.

5.1. Initial and eective stiness

5.1.1. Stiness obtained from vertical loading

The elastic modulus of the masonry E_m, when extracted from the simple compression tests carried out as part of the material tests, is equal to 5328 MPa (Table 2). Another way to obtain E_m that is reported in the literature [2], is to derive it from the first step of the shear-compression tests, when the axial force N is progressively applied to the wall (Section 2.6). Similarly to the former derivation, E_m is derived by linear fitting the unloading/reloading cycles that are conducted at three levels of the vertical force. At low levels of axial force, the deformation of the base and top mortar layers is still large compared to that of the wall. For this reason, E_m is extracted as in the former derivation, i.e by taking as base length 6 units and 6 mortar joints. This alternative method gives an average value of E_m of 3842 MPa (C.o.V. = 17 %), which is 28% lower than the value given by the former method. The elastic modulus derived from the first phase of the shear-compression tests considers vertical loading up to 15% of the axial load bearing capacity only while in the simple compression test the test unit was loaded up to compression failure. Deriving the elastic modulus from the secant stiness at 15% of the peak force from the simple compression tests gives E_m = 3378 MPa, which is very close to the value obtained from the first phase of the shear compression test.

For masonry walls of typology E, the Italian technical standard [12] proposes values of E_m between 2400 and 3200 MPa; considering these values as the 16th and 84th percentile values together with a lognormal distribution, an average of 2800 MPa is obtained [2].

5.1.2. Stiness obtained from horizontal loading

The present shear-compression tests show that the initial and eective horizontal stiness of the walls, together with the peak force, increase with the increase of the axial load ratio (Section 4.2). This finding was reported also in other test series on stone masonry walls [5, 4] and observed as a general trend in the analysis of a database containing tests from 16 campaigns [2]. The same trend is also known for brick masonry walls, as supported by several test series (e.g. [13, 14, 15]) and the analysis of a database containing tests from 7 campaigns [23]. The present test results show further that the number of applied cycles per drift demand aects the eective stiness only and not the initial one (Section 4.2). This observation is new as existing experimental data about the influence of the load history on the force-displacement behaviour of masonry walls is limited to the dierence between monotonic and cyclic loading only, and not on the number of applied cycles [6, 7, 5, 4]. Through numerical simulations, Wilding *et al.* [3] found that the load history does not influence significantly the peak force or the eective stiness of shear-controlled brick masonry walls.

The current version of the Eurocode 8 - Part 3 [24, Section C.3] assumes that the initial wall stiness can be computed using a Timoshenko-beam model in conjunction with an elastic and a shear modulus that are independent of the axial load ratio. Moreover, the eective stiness is computed as a ratio of the initial stiness. As such, this approach does not allow capturing the influence of the axial load ratio neither on the initial nor on the eective wall stiness.

Vanin *et al.* [2] proposed an expression for estimating the eective elastic modulus, indicated here with $E_{m,e}$, as a function of the axial load ratio $\square_v/f_{cm}$. The expression, which was obtained from linear regression of the database on stone masonry walls [2], reads:

$$E_{m,e} = \left(\frac{E_m}{f_{cm}}\right)_{ref} f_{cm} \frac{(\square_v/f_{cm})}{0{:}30}; \tag{1}$$

where f_{cm} is the compressive strength of masonry, taken equal to the mean value obtained from the material tests (Section 2.2) and $(E_m/f_{cm})_{ref}$ is a reference value which, is proposed to be equal to 200 for walls of typology E (lower bound) and 700 for typology A (upper bound) [2]. This expression, which can be used for calculating the eective stiness of an in-plane wall by modelling this latter as a Timoshenko beam, is compared here against the present

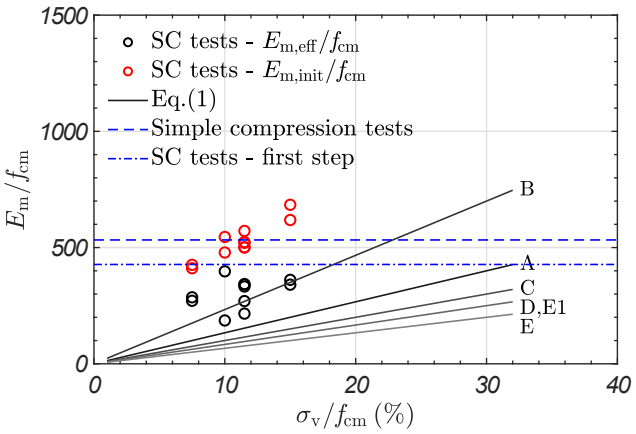

Figure 13: Normalized initial and eective elastic modulus of the masonry versus axial load ratio obtained from simple compression and shear-compression tests. For the eective elastic modulus, test values are compared to those given by Eq.(1) for dierent masonry typologies A-E1 [2]. For the cyclic tests, the moduli obtained both from the negative and from the positive cycles are plotted.

test results. For the comparison, an estimate of the experimental eective elastic modulus is obtained as described in Vanin *et al.* [2]. The wall is considered as a Timoshenko beam that is subjected to a horizontal force at its top and has a shear span $H_0 = H_w$=2, so that the initial wall stiness writes:

$$K_{init} = \left[\frac{H^3}{12E_m I_w} + \frac{6H_w}{5G_m L_w t_w} \right]^{-1}; \tag{2}$$

The experimental value of the initial elastic modulus is then obtained from the above expression as:

$$E_{m,init} = \frac{K_{init} H_w \left[6L_w^2 + 5H_w^2 \frac{G_m}{E_m} \right]}{5 t_w L_w^3 \frac{G_m}{E_m}}; \tag{3}$$

where the G_m=E_m ratio is set to 0.33 [2]. The experimental eective modulus $E_{m,e}$ is finally obtained as:

$$E_{m,e} = E_{m,init} \frac{K_e}{K_{init}}; \tag{4}$$

The Eurocode 8 - Part 3 [24, Section C.3] recommends a ratio between eective and initial stiness of 0.50, whereas the average value obtained from the present tests is 0.57 (Section 4.4), which is in line with the value given by the Eurocode 8 and very close to the average value of 0.59 (C.o.V. = 51%) obtained from the database on in-plane stone masonry walls failing in shear [2]. For the comparison, the ratio is evaluated with the value for K_e=K_{init} experimentally obtained for each wall.

Fig. 13 shows how the experimental values for $E_{m,init}$=f_{cm} vary linearly with the axial load ratio, while the data points of $E_{m,e}$=f_{cm} are more scattered, due to the variability observed in the K_e=K_{init} ratio (Section 4.4). Compared to Eq.(1), the set of values obtained for $E_{m,e}$=f_{cm} are close to the region of those predicted by the expression for walls of typology B but significantly higher than those of typology E. The figure also includes the values for E_m=f_{cm} obtained from simple compression tests on the walls and from the application of the vertical force in the first step of the shear-compression tests. These values are centered on the data points of the initial stiness $E_{m,init}$=f_{cm} obtained from the shear-compression tests.

5.2. Force capacity

The present tests show that the peak force increases linearly with the increase of axial load ratio but is not aected by the load history (Section 4.1). Current codes, which allow computing the peak force as a function of the axial force but do not consider the load history, capture these trends.

In the Eurocode 8 - Part 3 [24, Section C.4], the force capacity of a generic in-plane loaded masonry wall at the Severe Damage (SD) limit state is defined as the minimum among the forces corresponding to three possible failure modes, namely: V_f, corresponding to the flexural failure of the wall, V_s, corresponding to the shear failure of the wall and $V_{s;units}$, corresponding to the failure of the masonry units [24]:

$$V_{SD} = \min\{V_f\ ;\ V_s;\ V_{s;units}\}: \tag{5}$$

When applied to the present tests the above quantities are calculated as follows:

$$V_f = \frac{L_w N}{2H_0}\left(1 - 1{:}15\frac{N}{t_w L_w f_{cm}}\right)$$
$$V_s = c t_w L_c + \mu N$$
$$V_{s;units} = 0{:}065 f_{cb} t_w L_c;$$

with: L_w and t_w respectively the length and the thickness of the walls (Fig. 3); L_c the length of the assumed compressed region of the walls, estimated as $L_c = 3(L_w/2 - M/N)$ [25] and with M equal to the moment applied at the top of the walls when the peak horizontal force V_{max} is reached: $M = V_{max}H_0$; H_0 the shear span, equal to $1/2H_w$ (Fig. 3); N the vertical axial force acting on the wall top; f_{cm} and f_{cb} respectively the compressive strength of masonry and the compressive strength of the units, herein taken equal to the mean values obtained from the material tests (Section 2.2); μ the characteristic friction coefficient of masonry, and c the characteristic shear strength of masonry, calculated in the absence of vertical forces and therefore representative of the overall wall cohesion. In the absence of any other clear indication, μ can be set to 0.4 [24] and estimates of c are between 0.09 and 0.12 MPa for masonry of typology E [12]. These values are here benchmarked against those obtained by fitting the expression for V_s on the experimental results.

Another expression that is often used for estimating the force capacity of walls failing in shear [2] is given by the Turnšek-Čačovič failure criterion [26], which is here expressed as:

$$V_{TC} = \frac{t_w L_w}{b} f_t \sqrt{1 + \frac{N}{t_w L_w}\frac{1}{f_t}}; \tag{6}$$

with the factor b modelling the distribution of the shear stresses along the middle section of the wall, here set equal to $H_w/L_w = 1$ [2], and f_t the masonry tensile strength. For masonry walls of typology E, an indication of f_t is 0.16 MPa [2], whereas $f_t = 0{:}11$ MPa was obtained from the diagonal compression tests (Section 2.2). As for μ and c, also f_t is here back-calculated by fitting the the expression for V_{TC} on the test results.

In Fig. 14, the expressions for the force capacity V_f calculated using the experimental value of f_{cm}, the expressions for V_s and V_{TC} resulting from fitting, and the peak force V_{max} obtained from the tests are compared. The expression for $V_{s;units}$ gives a value of 550 kN which is outside the plotting range and therefore not visible in the figure. The expressions given by the Eurocode 8 predict correctly that all walls fail in shear, because V_f is higher than V_s. The values for μ and c back-calculated from the diagram by fitting a linear relationship to the data points are $\mu = 0{:}47$, corresponding to a characteristic friction angle of 25°, and $c = 0{:}07$ MPa. This latter is found by setting L_c equal to 650 mm, which is the average compressed length calculated for all the tests. The values obtained for c and μ are very close to those suggested in the codes and the criterion seizes very well the experimental trend observed in the range of axial loads investigated in the campaign.

The Turnšek-Čačovič criterion, which is also fitted on the test results, gives a best-fit value for f_t of 0.25 MPa that is higher than what observed from the diagonal compression tests and proposed in the codes. Moreover, fitting this criterion in this range of investigated axial loads leads to an over- and underestimation respectively in the lower and upper range of investigated loads.

5.3. Drift limits

Results from the present tests show that the sensitivity of the drift limits to the axial load ratio and load history varies (Section 4.3). Higher values of axial load result in lower values of ultimate drift θ_u and drift at collapse θ_c, and higher values of θ_y, while the other drift limits θ_{cr}, θ_{max} and θ_{SD} are not significantly influenced by the axial load ratio.

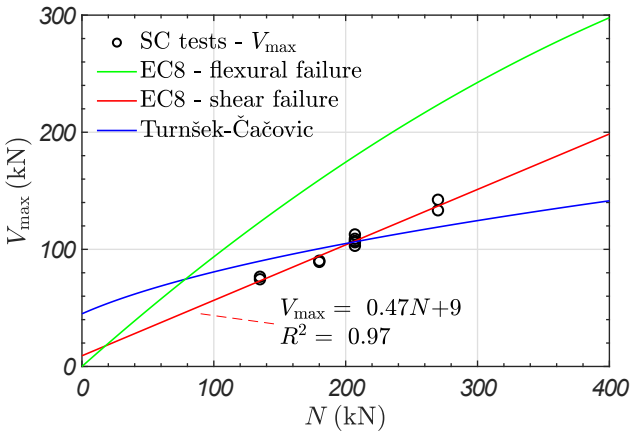

Figure 14: Shear force-axial force diagram comparing the peak force obtained from the shear-compression tests with the force capacity fitted according to the expressions contained the Eurocode 8 - Part 3 [24, Section C.4], Eq.(5), and to the Turnšek-Čačovič criterion [26], Eq.(6). For the cyclic tests, the peak forces obtained both from the negative and from the positive cycles are plotted.

The trends observed for $\square_{cr}$, $\square_u$ and $\square_c$ are in line with the observations derived from the database on stone masonry walls [2].

With regard to the eect of the load history, all the drifts, especially the ultimate drift $\square_u$ and the drift at collapse $\square_c$, are very sensitive to the number of cycles per drift level and, in particular, decrease when this number increases. Previous tests showed that cyclic tests lead to about half the ultimate drift $\square_u$ when compared to monotonic tests [2]. This result is confirmed by numerical simulations of shear-controlled unreinforced brick masonry walls [3] and is in line with the results of this test series, where all walls fail in shear and the ratio between the ultimate drift from cyclic (SC5) and monotonic loading (SC7) is 0:56. The numerical simulations further investigated asymmetric load histories and showed that such load histories lead to ultimate drifts that are in between those of monotonic and symmetric, or fully reversed, cyclic loading [3]. Would have SC6 been subjected to the intended symmetric load history with 100 cycles per drift rather than the asymmetric one, the decrease in ultimate drift with increasing number of cycles, i.e. between SC6 and SC5, might have been therefore stronger than the observed ratio of 0.80. The numerical simulations in [3] only considered cyclic load histories with up to 3 cycles per drift level and the eect of a high number of cycles was not investigated.

The Eurocode 8 - Part 3 [24, Section C.4] defines drift values that are independent of the axial load ratio and of the load history but depend on the wall failure modes. For walls undergoing shear failure, the drift at the Severe Damage limit state $\square_{SD}$ is equal to 0.4% and the drift at the Near Collapse limit state $\square_{NC}$, corresponding here to the drift at collapse $\square_c$, as $4=3\square_{SD} = 0:53\%$. When compared with the present test values (Section 4.3), $\square_{SD} = 0:4\%$ is an upper bound for almost all tested walls (Fig. 10(d)), while $\square_{NC} = 0:53\%$ is visibly a lower bound for all tests (Fig. 10(f)).

Based on the analysis of the database on stone masonry walls, Vanin *et al.* [2] proposed an equation linking the ultimate drift $\square_u$ to the axial load ratio and the shear span of the wall. For walls of typology E and E1, the equation reads:

$$\square_u = \max\{1:5\% \quad 4\%\frac{\square_v}{f_{cm}}; 0:3\%\}\frac{H_0}{\min\{L_w; H_w\}}: \tag{7}$$

To obtain an equation for walls of typologies A to D, 1.5, 4, 0.3% are replaced with respectively 2.25, 6 and 0.45% in the above expression. The drift at the onset of cracking of masonry is taken as $\square_{cr} = 0:20\%$, whereas the drifts at the other limit states are expressed as a fraction of the ultimate drift as [2]:

$$\begin{aligned}
\square_y &= 0:25\square_u \\
\square_{SD} &= 0:5\square_u \\
\square_{max} &= 0:7\square_u \\
\square_c &= 1:15\square_u:
\end{aligned} \tag{8}$$

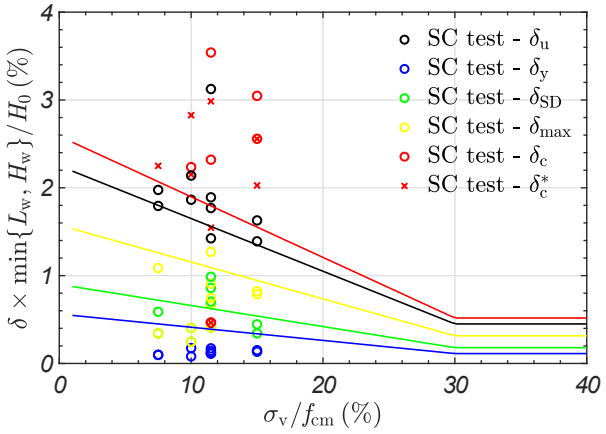

Figure 15: Normalized drifts versus axial load ratio. Comparison between test values (data points) and trends given by Eq.(7)-(8) for masonry of typology E-E1 [2] (solid lines). For the cyclic tests, the drifts obtained both from the negative and from the positive cycles are plotted.

Table 7: Ratio of collapse drift estimated as the drift measured at 50% drop in the peak force (δ_c^*) to the collapse drift at which the axial load-bearing capacity is lost (δ_c). Mean and C.o.V. are calculated based on all values obtained from the positive and the negative envelope curves.

Test	δ_c^*/δ_c	
	pos.	neg.
SC1	0.75	0.46
SC2	0.96	0.58
SC4	1.00	0.67
SC5	0.84	1.00
SC6	1.00	0.67
SC7	0.40	-
Mean	0.76	
C.o.V.	29%	

As shown in Fig. 15, Eq.(7)-(8) allow estimating with good precision the experimental drift values, with, in general, an underestimation of the wall drift capacity and a slight overestimation of the yield drift. The estimate for δ_{cr} of 0.20% is approximately twice as high as the average values observed in the tests. The equation for the drift capacity δ_c was calculated, for the tests in which the walls were not tested up to failure of the vertical load-bearing capacity, as the drift at 50% drop of the peak force [2]. Applying this definition to the present tests, see δ_c^* in Fig. 15, lead to values that are lower than δ_c and are slightly closer to Eq.(8). As shown in Table 7, using δ_c^* rather than δ_c leads, in general, to an underestimation of the drift capacity of the walls.

6. Conclusions

The experimental test programme reported in this paper investigated the force-displacement behaviour of plastered stone masonry walls made of regular sandstone blocks under shear-compression loading. According to the classification drafted in the Italian technical standard [12] and detailed in [9, 2], the tested walls were representative of typology E stone masonry.

The campaign investigated the influence of the axial load ratio and the load history on the stiness, strength and drift parameters of the walls. It confirmed previous findings with regard to the influence of the axial load ratio, showing that, with increasing axial load ratio, the initial stiness and the force capacity of the walls increase, whereas the ultimate drift decreases. It also showed that the load history has negligible influence on the stiness and the force capacity of the walls; on the contrary, the ultimate drift was observed to be very sensitive to the load history, being

larger when the walls were subjected to a monotonic loading than when they were subjected to a cyclic loading. As shown in the paper, this is also in line with previous experimental and numerical studies. In addition to previous studies, this campaign investigated also the eect of the number of cycles per drift demand, which was increased from 2 to 100. The number of cycles applied per drift demand lead to an important decrease of not only the ultimate drift of the walls but, more generally, of all the drift measures corresponding to the considered wall limit states. From all the tests, the collapse drift, i.e. the drift corresponding to the loss of wall axial load-bearing capacity, was measured, showing that considering the drift measured at 50% drop in the peak force leads to an underestimation of the actual wall displacement capacity.

The presence of plaster on one face of the walls enabled finding a correlation between the onset of cracking in the plaster with the cracking of the stone masonry wall. Finding this correlation is of interest for the seismic assessment of historical buildings, as it can be used for the definition of limit states of artistic assets connected to the structural elements [9, 10]. On the basis of the obtained experimental test results, it can be assumed that the plaster cracks at the same drift level than the masonry wall. There is a small indication that the cracking of plaster occurs before the cracking of the masonry when the number of cycles performed in the load history increases, but the data is not yet su□cient to build a robust model.

Acknowledgments

The first two authors of this study as well as the plastering of the walls were financed through the research grant 'Assessment of historical stone masonry buildings when subjected to ground motions of short return period' by the Swiss Federal O□ce for the Environment (OFEV), the Swiss Federal O□ce of Culture (OFC) and the Swiss Federal O□ce of Civil Protection (OFPP). The third author and the construction of the walls were supported by the Swiss National Science Foundation through the grant 200021_140973/1. The authors would like to thank the team of the Structural Engineering Laboratory at EPFL for their technical support. Thanks also go to the students who helped with the tests, in particular to the four Master students Daniel Grueter, Nathan Richard, Elsa Englade and Dionysia Michalogianni.

References

[1] G. Grünthal, Cahiers du Centre Européen de Géodynamique et de Séismologie: Volume 15 — European Macroseismic Scale, Tech. rep., Luxembourg (1998).

[2] F. Vanin, D. Zaganelli, A. Penna, K. Beyer, Estimates for the stiness, strength and drift capacity of stone masonry walls based on 123 quasi-static cyclic tests reported in the literature, Bulletin of Earthquake Engineering (2017) 1–37 doi:10.1007/s10518-017-0188-5. URL http://link.springer.com/10.1007/s10518-017-0188-5

[3] B. V. Wilding, K. M. Dolatshahi, K. Beyer, Influence of load history on the force-displacement response of in-plane loaded unreinforced masonry walls, Engineering Structures 152 (2017) 671–682. doi:10.1016/j.engstruct.2017.09.038. URL https://doi.org/10.1016/j.engstruct.2017.09.038

[4] F. F. Pinho, V. J. Lúcio, M. F. Baião, Rubble stone masonry walls in Portugal strengthened with reinforced micro-concrete layers, Bulletin of Earthquake Engineering 10 (1) (2012) 161–180. doi:10.1007/s10518-011-9280-4.

[5] G. Vasconcelos, P. B. Lourenc¸o, In-Plane Experimental Behavior of Stone Masonry Walls under Cyclic Loading, Journal of Structural Engineering 135 (10) (2009) 1269–1277. doi:10.1061/(ASCE)ST.1943-541X.0000053. URL http://ascelibrary.org/doi/10.1061/{%}28ASCE{%}29ST.1943-541X.0000053

[6] H. Ganz, B. Thürlimann, Versuche an Mauerwerksscheiben unter Normalkraft und Querkraft, Tech. rep., ETH Zurich, Zurich (1984).

[7] G. Magenes, G. M. Calvi, Cyclic behaviour of brick masonry walls, in: Proceedings of the 10th World Conference of Earthquake Engineering, Rotterdam, 1992.

[8] M. Tomaževič, M. Lutman, L. Petkovič, Seismic behavior of masonry walls: experimental simulation, Journal of Structural Engineering 122 (9) (1996) 1040–1047.

[9] M. Krzan, S. Gostic, S. Cattari, V. Bosiljkov, Acquiring reference parameters of masonry for the structural performance analysis of historical buildings, Bulletin of Earthquake Engineering 13 (1) (2015) 203–236. doi:10.1007/s10518-014-9686-x.

[10] C. Calderini, S. Degli Abbati, P. Cotič, M. Krzan, V. Bosiljkov, In-plane shear tests on masonry panels with plaster: correlation of structural damage and damage on artistic assets, Bulletin of Earthquake Engineering 13 (1) (2015) 237–256. doi:10.1007/s10518-014-9632-y.

[11] P. Cotič, Z. Jagličić, V. Bosiljkov, Validation of non-destructive characterization of the structure and seismic damage propagation of plaster and texture in multi-leaf stone masonry walls of cultural-artistic value, Journal of Cultural Heritage 15 (5) (2014) 490–498. doi:10.1016/j.culher.2013.11.004.

[12] CNTC2009, Circolare 02/02/2009 n. 617. Istruzioni per l'applicazione delle "Nuove norme tecniche per le costruzioni" di cui al Decreteo Ministeriale 14/1/2008. Gazzetta U□ciale della Repubblica Italiana n. 47, Supplemento Ordinario n. 27 (in Italian).

[13] V. Bosiljkov, Y. Totoev, J. Nichols, Shear modulus and stiness of brickwork masonry: An experimental perspective, Structural Engineering and Mechanics 20 (2005) 21–43. doi:10.12989/sem.2005.20.1.021.

[14] S. Petry, K. Beyer, Influence of boundary conditions and size eect on the drift capacity of URM walls, Engineering Structures 65 (2014) 76–88. doi:10.1016/j.engstruct.2014.01.048.
URL http://dx.doi.org/10.1016/j.engstruct.2014.01.048
[15] A. H. Salmanpour, N. Mojsilovi´c, J. Schwartz, Displacement capacity of contemporary unreinforced masonry walls: An experimental study, Engineering Structures 89 (2015) 1–16. doi:10.1016/j.engstruct.2015.01.052.
[16] A. Moropoulou, A. Bakolas, S. Anagnostopoulou, Composite materials in ancient structures, Cement and Concrete Composites 27 (2) (2005) 295–300. doi:10.1016/j.cemconcomp.2004.02.018.
URL http://linkinghub.elsevier.com/retrieve/pii/S0958946504000356
[17] Vitruvius, Ten Books on Architecture (English version), Harvard University Press, Cambridge, 1914.
[18] EN 1015, Methods of test for mortar for masonry-Part 11 Determination of flexural and compressive strength of hardened mortar (2000).
[19] ASTM D7012 - 10, Standard test method for compressive strength and elastic moduli of intact rock core specimens under varying states of stress and temperatures (2010).
[20] A. Brignola, S. Frumento, S. Lagomarsino, S. Podestá, Identification of shear parameters of masonry panels through the in-situ diagonal compression test, International Journal of Architectural Heritage 3 (1) (2009) 52–73. doi:10.1080/15583050802138634.
[21] A. Borri, M. Corradi, G. Castori, A. De Maria, A method for the analysis and classification of historic masonry, Bulletin of Earthquake Engineering 13 (9) (2015) 2647–2665. doi:10.1007/s10518-015-9731-4.
URL http://dx.doi.org/10.1007/s10518-015-9731-4
[22] Correlated Solutions, Vic-3D 7 (2016).
[23] B. V. Wilding, K. Beyer, Analytical and empirical models for predicting the drift capacity of modern unreinforced masonry walls, Earthquake Engineering & Structural Dynamics 47 (10) (2018) 2012–2031. doi:10.1002/eqe.3053.
URL http://doi.wiley.com/10.1002/eqe.3053
[24] CEN, Eurocode 8: Design of structures for earthquake resistance, Part 3: Assessmemtand retrofitting of buildings, Tech. Rep. EN 1998-3, Brussels (2005).
[25] S. Petry, K. Beyer, Force-displacement response of in-plane-loaded URM walls with a dominating flexural mode, Earthquake Engineering & Structural Dynamics 44 (14) (2015) 2551–2573. doi:10.1002/eqe.2597.
URL http://onlinelibrary.wiley.com/doi/10.1002/eqe.2230/fullhttp://doi.wiley.com/10.1002/eqe.2597
[26] V. Turnšek, F. Čačovič, Some experimental results on the strength of brick masonry walls, in: Proceedings of the 2nd International Brick Masonry Conference, Stoke-on-Trent, England, 1971, pp. 149–156.
URL http://www.hms.civil.uminho.pt/ibmac/1970/149.pdf